LUND UNIVERSITY
Faculty of Science

sol voltaics™

Alignment and Orientation of Nanowires in a Thin Film under the Influence of an Electric Field

Sara Thorberg

Thesis submitted for the degree of Master of Science in Physics, Nanoscience

Project duration: 4 months

Supervised by Martin Magnusson and Per Viklund

Department of Physics
Division of Solid State Physics,
and Sol Voltaics
May 2016

Abstract

The demand for cheaper and more efficient solar cells is high. One way to decrease cost of material, while maintaining a high degree of efficiency, is to take advantage of nanomaterials. A thin film containing *pn*-junction nanowires can convert light with an efficiency comparable to traditional planar cells, while using a fraction of the material, and thus reduce costs.

At the company Sol Voltaics, a tool for mass producing solar cell nanowires, called Aerotaxy, is used. This method uses aerosol seed particles to grow nanowires, as they flow through a heated pipe. The resulting, randomly distributed, nanowires need to be arranged in arrays such that they can be contacted and used to convert light to electricity. This project focuses on a method to achieve this by using an external electric field.

The solar cell nanowires contains a dipole moment due to their *pn*-junction. When an external electric field is applied over the nanowires, there is an interaction between the field and the dipole. An additional dipole moment is generated in the nanowire under the influence of the electric field, due to the polarization in the material. The junction dipole is directional in the sense that the plus pole and the minus pole is set, while the direction of the polarization dipole will depend on the position of the nanowire relative to the electric field. These two effect also have different dependence on the electric field strength. Therefore, it is here proposed that the degree of orientation of the aligned nanowires depends the strength of the applied field. The aim of this project was to realize the relative magnitude of the junction dipole and the polarization dipole. This was done by a combination of computations and experiments.

Modeling of the nanowire dipoles in an electric field show that all nanowires should orient for field strength below 0.26 V/μm, after which the polarization effect becomes dominant, resulting in decreasing orientation among the nanowires. In order to reach alignment, on the other hand, a higher field strength is required.

Thin films of *pn*-junction nanowires in PDMS were produced under the influence of an applied DC electric field. Results indicate a preferred direction of the nanowires in the electric field. However, higher field strengths were required for alignment of the nanowires, than was predicted from computations. The difference in field strength required for orientation of nanowires compared to alignment of nanowires creates a problem. The proposed solution to this problem is a gradually increased electric field strength.

Acknowledgments

I would like to express my sincere gratitude to my supervisors Martin Magnusson and Per Viklund for their support and advisement throughout my thesis project, and for patiently proof-reading the report. They have given me great advice and guidance throughout the experiments, without which, this thesis project would not have been as rewarding.

I am also grateful to Mikael Björk, Ingvar Åberg, and Omid Madani for the rewarding discussions and input regarding modeling and simulations, and to Jaime Castillo-León for the guidance in the experimental work. I am very thankful to have had such knowledgeable people available.

Finally, I would like to thank my boyfriend Robin Westlund, who at least made an effort to proof-read my report, even though he only made it through the introduction.

List of acronyms and abbreviations

AlAs	aluminum arsenide
GaAs	gallium arsenide
GaN	gallium nitride
Ge	germanium
InP	indium phosphide
ITO	indium tin oxide
MOCVD	metal-organic chemical vapor deposition
NW	nanowire
PDMS	polydimethylsiloxane
PV	photovoltaic
PVA	polyvinyl alcohol
SEM	scanning electron microscopy
Si	silicon

Contents

1 Introduction

The need to increase the use of renewable energy sources has never been as critical as it is now. With the rising levels of carbon dioxide in the atmosphere and all the effects caused by increasing temperatures, it is urgent to replace the burning of fossil fuels. There are many available candidates to meet these needs, from wind power plants to bio gas. However, the two mentioned examples are only indirect sources of energy that originate from the Sun. The light from the Sun heats up the air in our atmosphere, causing streams that can be used to drive a windmill generator. Plants use the light to grow complex biological structures that we can use for combustion. One way to use the energy from the incoming light more efficiently is to collect it directly and convert it to electricity in photovoltaic (PV) solar cells.

The semiconductor PV cells is a rapidly expanding part of the solar industry, with a compound annual growth rate of 44 % during the years 2000–2013.[1] The reason for the success of the PV cells can be accredited to its high efficiency, relative to other alternatives, the abundance of silicon, which was the material used in 90 % of the production in 2003,[1] and since the production technology of semiconductor devices is well established. Out of the semiconductor materials the III-V compounds, such as gallium arsenide (GaAs) and indium phosphide (InP), have properties which yield a higher efficiency energy conversion from light than group IV materials, such as silicon (Si). Therefore, GaAs has become a popular material to use for high efficiency solar cells. However, GaAs is more expensive than the more abundant Si, and it is therefore interesting to find a way to minimize the material used, while maintaining the high efficiency. Using an array of PV nanowires (NWs) would allow a high efficiency while using only a fraction of the material required for planar solar cells, due to the waveguide effect that occurs as light is incident on the nanowire array. In addition to the lower amount of material used, a new technique to producing nanowires have been developed at Lund University and Sol Voltaics, called Aerotaxy. In Aerotaxy, nanowires are grown from gold seed particles as they flow through a hot furnace, enabling a fast and continuous production.

1.1 Background

Like many other semiconductor devices, the silicon solar cell was invented at Bell Laboratories (at least the first solar cells that could produce any significant amount of power). There had been previous observations of photovoltaic current between metal electrodes in an electrolyte solution, by Alexandre-Edmond Becquerel, as early as 1839. The first real advance in the field occurred when a *pn*-junction, i.e. an interface between two semiconductor regions with different doping, was created in a silicon sample at Bell Laboratories in 1940. Daryl Chapin, Calvin Fuller, and Gerald Pearson worked on improving the control of different impurities in silicon in order to increase the efficiency of the cell. In 1954 they presented a solar cell with 6 % efficiency.[2]

Another large driving force in technology development is the space industry, which took developed the solar panels further to use for space vehicles and satellites. Such devices required predictable energy supply during a long time without the need for maintenance, since they are far from reach and power grid. Solar cells could supply this with a life span of 5–10 years.[3] It was not until the 70's that solar cells started to be considered as an alternative power supply. Although an interesting candidate, the cost of the crystalline silicon cells still needed to be drastically reduced in order to become commercially competitive.

Since then, many different approaches have been made to increase the efficiency and reduce the cost of solar power. Silicon has been exchanged for gallium arsenide in high efficiency solar cells, although at the cost of higher prices, and mainly used in space. At other end of the price range are the low cost, and less efficient, thin film cells. These thin film solar cells can be added onto a glass or metal substrate, or in tandem with another solar cell, which pushes the power yield even further. Due to innovations in the solar cell industry, the cost per watt has been reduced. However, further development is needed in order to combine high efficiency and low cost. This is where nanowires come into the picture.

At Sol Voltaics, a thin film solar cell is developed which contains arrays of p-n junction GaAs nanowires.[4] Due to a high throughput growth method, called Aerotaxy, high quality nanowire can be produced at a low cost. In addition, the nanowire cell can convert light to electricity at

an efficiency of 15.3% , although the nanowire array is only covering 13% of the surface area.[5] The high efficiency of the cell can be credited to the optoelectronic properties of the semiconductor compound GaAs, as well as the waveguide effect that occurs as the light reaches the nanowire covered surface. The cell will function as an add-on to a planar silicon crystal solar cell and will increase past the theoretical limits for a silicon cell without an add-on. The cell on which the measurements were done contained nanowires grown with metal-organic chemical vapor deposition (MOVCD). During this process, the nanowires are grown on a wafer and the resulting arrays of nanowires in a pattern that can be controlled. However, work is being done towards a processing method where the efficient growth method Aerotaxy is used to produce the nanowires.[6] For the conversion from MOCVD to Aerotaxy-grown nanowires, an additional processing step is required, where the nanowires are arranged in ordered arrays.

Research has been done on a wide range of methods to assemble nanowires in different constellations by using external fields. Crassous et al. have used an AC field to assemble ellipsoidal nanorods into tubular shapes.[7] Troppenz et al. have investigated the angular distribution of silica rods under the influence of an electric field,[8] and Kim et. al. have investigated the movement of charged nanowires in an electric field.[9]

1.2 Aim of the project

The aim for this project was to understand how an electric field can be used to assemble nanowires in such a way that they can be contacted and perform as a solar cell. The method that is explored here takes advantage of the inherent charge distribution in nanowires containing a p-n junction in order to rotate them to alignment under the influence of a DC electric field.

Producing nanowires with the growth method Aerotaxy, results in a powder with randomly distributed nanowires, as illustrated to the left in figure 1. For the solar cell to produce current under illumination, the nanowires need to be arranged in arrays, all of them pointing in the same direction (right in figure 1), so that contacts can be efficiently attached to the ends of the wires.

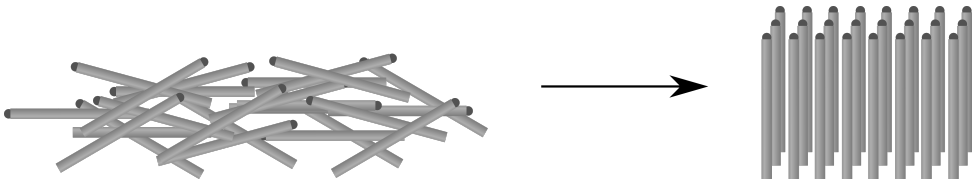

Figure 1

When producing a device which contains nanomaterials, the processing method needs to be treated differently than when working with macroscopic parts. One of the difficulties is not being able to distinguish the nanostructures with the naked eye. Instead, a microscope is required, either optical for an overview image, or an electron microscope for a detailed view. Another big challenge when working with nanoscale objects is the assembly of the pieces. The high efficiency obtained by Åberg et al.[5] required a nanowire density of about six million nanowires per square millimeter!. Because of the large number of wires necessary to reach high absorption, a method to assemble the nanowires in an effective and systematic way is required. The processing method does not only need to have a high throughput, but it also needs to be compatible with the rest of the steps in the production, and it needs to be reliable and reproducible to yield a high quality product.

There are a couple of terms which are frequently used throughout this report, and that therefore deserve proper clarification. The first term, *alignment*, or *aligned NWs*, refers to NWs that are parallel to each other and to the electric field lines. They do not need to be parallel in one line, as the image in figure 2a might suggest, although they can vary in height above a two-dimensional plane perpendicular to the electric field lines. The direction in which the NWs point is not relevant either for the alignment. They can point either up or down. The second term, *orientation*, or *oriented NWs*, refers to NWs whose seed particles also point in the same direction as each other, as illustrated in figure 2b.

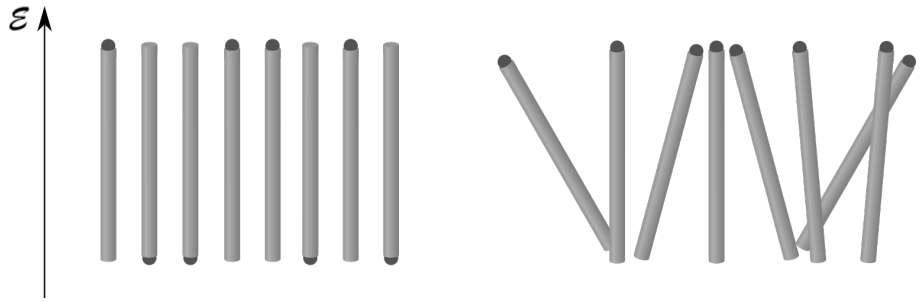

(a) Aligned NWs. *(b) Oriented NWs.*

Figure 2: Explanatory images for the terms aligned (a) and oriented (b) NWs.

The requirements on the wires, that have been used in this project, are listed below.

Alignment: NWs have an angle, θ, relative to the electric field within the range $0 < \theta < 0.1\pi$, or $0.9\pi < \theta < \pi$, since there is no regard to direction.

Orientation: NWs have an angle within the range $0 < \theta < 0.5\pi$.

In order for both conditions to be met, the NWs must have an angle within the range $0 < \theta < 0.1\pi$.

This project is based on the hypothesis that the charge separation around the junction between an *n*-doped and a *p*-doped region gives the nanowire properties of an electric dipole. Therefore, when the NW is exposed to an external field, the interaction between the field and the charges in the wires will exert a torque on the nanowire. However, the nanowires do not need the *pn*-junction to align with the field. The induced polarization in the material when it it is exposed to an electric field (DC or AC) will have this effect of *alignment* as well, figure 3a. However, since the polarization is independent of the *pn*-junction, the rotation due to polarization has no regard to direction, and will therefore not result in *oriented* nanowires. Thus, it is not obvious what would occur in the case where the nanowire has an initial direction anti-parallel to the field lines (figure 3b). The investigation in this thesis will therefore focus on the relative strength of these two effects. This will be done through theoretical and numerical modeling of the interactions between the charges in the material and the external field, as well as through experiments, to test the degree of orientation and alignment for different field strengths.

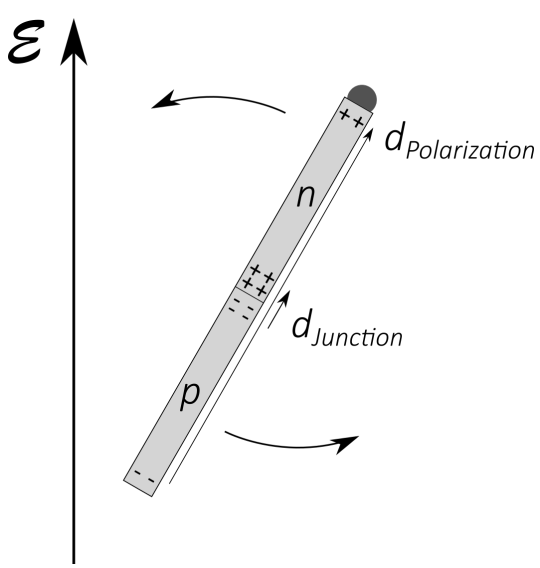

(a) In the case where two dipole moments are in the same direction, the NW will become oriented.

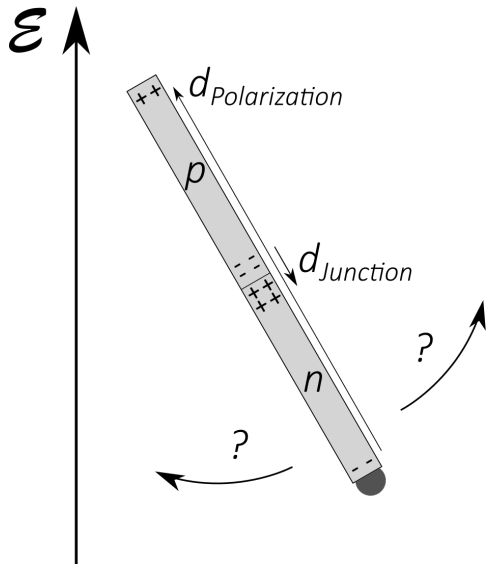

(b) If the NW has an initial direction such that the NW dipoles are opposite, it is not obvious how the NW will align.

Figure 3: Effect from moment exerted on the nanowires under the influence of an external electric field, depending on initial orientation of the NW relative to the field.

1.3 Structure of the report

The report start with a section on the behavior of the electrical charges in semiconductor materials, and the implications this has on the properties and possibilities of such materials. The purpose of this section is to understand the origin of the pn-junction, which is central for this project. The thesis project included two separate parts, which were performed in parallel. These two parts have been kept separate in this thesis, each with sections on method, results, and discussion. Part one (section 3) reviews the modeling part of the project, and part two (section 4) considers the experimental execution. The report ends with conclusions and outlook, common for the two parts.

2 Electrical Charge in Semiconductors

The hypothesis presented in the introduction depends on a non-constant charge distribution in the nanowires, which gives rise to a dipole moment that can interact with an electric field. This section gives an introduction to the electrical charges in semiconductors, and in particular how they give rise to the charge separation around the pn-junction. In order to understand the properties of the p-n junction, it is necessary to give a brief introduction to semiconductor physics, and especially how the energy bands of semiconductors affect the conduction properties, as well as the optical properties, of the material. In the final part of this section, the p-n junction is introduced.

2.1 Semiconductor materials

In the periodic table, there are three groups of solid materials - metals, insulators, and semiconductors. What distinguishes the three types of materials is their conductivity. Insulators have the lowest conductivity ($\sigma < 10^{-8}$ S/cm), metals the highest ($\sigma > 10^{3}$ S/cm), and semiconductors have a conductivity somewhere in between.[10] The difference in the ability to conduct current origins from the properties of the energy bands, and especially the two bands which are highest in energy: the valence and conduction bands. For pure (free of contaminations) insulators and semiconductors in the ground state, all states in the valence band are occupied and the conduction band is empty. This means that there are no free electrons that can conduct a current. The reason the materials are not completely insulating is that there are, in general, contaminations in the materials, as well as thermal excitation of electrons to the conduction state. The amount of thermally excited electrons depend on the size of the energy gap between the valance and the conduction band. What is special about semiconductors is that their conductivity can be easily altered with temperature, illumination, and by addition of contaminations, called *dopants*. We will investigate further what role the energy bands play for the properties of the material in section 2.2. Metals have a much higher conductivity, which can be credited to the one of two effects. In some cases the conduction band is overlapping with the valence band, which means that electrons can move freely between the them. An other case is that the outermost band is *partially* filled with electrons.

Examples of semiconductor materials are the group IV materials silicon (Si) and germanium (Ge), and the III-V compounds gallium arsenide (GaAs) and gallium nitride (GaN). All these semiconductor materials have, on average, four valence electrons per atom. This results in four covalent bonds for each atom with its surrounding neighbors. The crystalline structure of the bonded atoms usually take the form of diamond (Si, Ge), zinc blende (GaAs), or wurtzite (GaN).

2.2 Energy Bands

The energy bands form when individual atoms, each with a set of energy levels, are brought together to form a crystal. It is the interaction between the discrete energy levels of the huge amount of atoms in the material that forms continuous bands of energy states, with *bandgaps*, i.e. ranges of energies that do not contain any states, in between. Most important are the highest band which is occupied by electrons, the *valence band*, and the lowest unoccupied band, the *conduction band*. It is the occupation and form of these bands that determine the conducting properties of a material. As previously mentioned, semiconductors have a completely filled valence band (at zero temperature and thermal equilibrium) and an empty conduction band. The size of the bandgap of a semiconductor on the order of 1 eV,[10] which should be viewed in relation to the thermal energy at room temperature, $kT = 26\,\text{meV}$.

2.2.1 Direct and indirect bandgap

In this project the optoelectronic properties of the semiconductor are important, involving the transitions that occur when the material is illuminated. For optical transitions, it is not only the size of the bandgap that matters, but also the shape of the bands.

There are two types of semiconductors: direct bandgap semiconductors, and indirect bandgap semiconductors. Direct bandgap semiconductors have the maximum point of the valence band and the minimum of the conduction band for the same wave vector, usually at $\boldsymbol{k} = (0, 0, 0)$. This means that a transition with the lowest required energy does not require a change in $\boldsymbol{k}$. For the indirect bandgap this is not the case, instead the minimum of the conduction band is usually at some point at the end of the Brillouin zone (see the Kittel[11] textbook on solid state physics

for more details on the Brillouin zone). This affects the transition probability between the two bands. For light is the wavevector related to the momentum as $\boldsymbol{k} = \boldsymbol{p}/2\pi$, where the magnitude of the momentum is related to energy as $p = E/c$. The wavevector of a photon with energy in the order of the transition energy (~ 1 eV) is thus very small, so an absorbed photon results in a vertical transition in the energy-wavevector diagram, as illustrated in figure 4a. In order for a transition as illustrated in figure 4b to occur in a semiconductor with an indirect bandgap, some additional wavevector need to be added. This is in general achieved through interaction with lattice vibrations, or *phonons*. Since the interaction with the photon and the phonon must be simultaneous (within the time-energy uncertainty), this greatly reduces the probability of the transition. Due to its direct bandgap, the semiconductor compound GaAs has a larger absorption coefficient, and thus work better as a solar cell, than the group IV element Si, which has an indirect bandgap.[12]

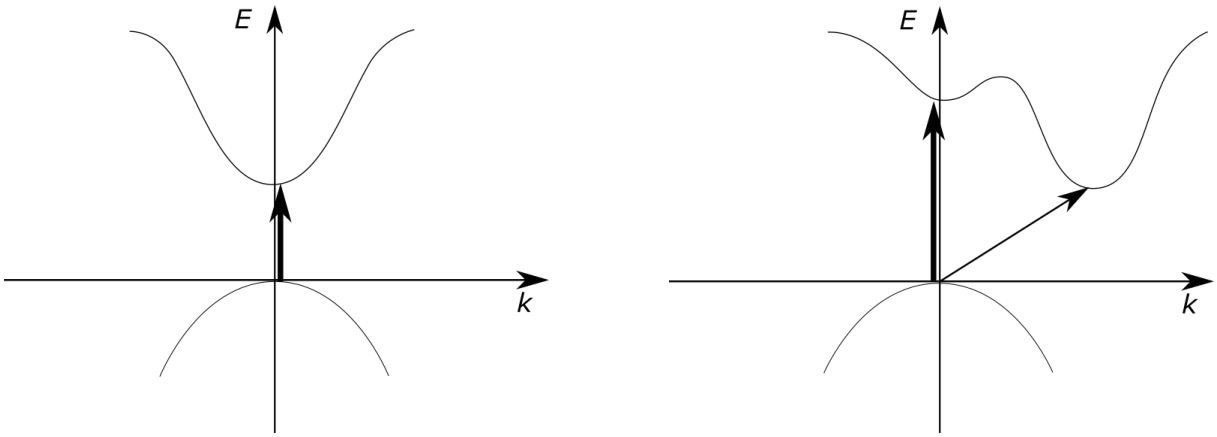

(a) Direct bangdap. *(b) Indirect bandgap*

Figure 4: Sketch of band structure for a direct (a) and indirect (b) semiconductor. The arrows illustrate possible transition, where the thickness indicate the probability of the transition.

2.3 Charge Carrier Concentration

The term *charge carrier* refer to the free electrons, i.e. occupied states in the conduction band, and free holes which are unoccupied states in the valence band. It is the charge carriers that will drift when an external field is applied, and thus give rise to a current. If the temperature is at absolute zero, a semiconductor material would have no charge carriers to create a current. However, in most cases the temperature is not at absolute zero. Therefore, rather than having the system in a ground state, there will be a thermal distribution of electrons, where the probability

for a state with energy, E, is given by the Fermi distribution function:

$$f(E) = \frac{1}{e^{(E-E_F)/kT} + 1} \tag{1}$$

The probability of occupation decreases exponentially for states with *E* larger than the Fermi energy level, E_F, and how fast the decay is depends inversely on the thermal energy kT. For a pure semiconductor in thermal equilibrium the Fermi energy will be right in the middle of the band gap. The probability to have thermally excited charge carriers is thus higher for smaller bandgaps, which could be expected. The electron concentration in the conduction band is calculated by integrating the product between density of states, i.e. the number of electron states per unit volume, and the Fermi function, i.e. the probability of that state being occupied by an electron, over the energies of the conduction band.

$$n = \int_{E_C^{bottom}}^{E_C^{top}} f(E)\, D(E)\, dE \tag{2}$$

A similar calculation can be done to calculate the concentration of holes in the valence band. In that case, $1 - f(E)$ is used, which is the probability of a state to be unoccupied, and the integration is done over the energies of the valence band. For an intrinsic semiconductor, the electron concentration in the conduction band is equal to the hole concentration in the valence band. If this is the case, the *intrinsic carrier concentration* for both holes and electrons can be derived as:[10]

$$n_i = \sqrt{N_C N_V}\, e^{-E_g/2kT} \tag{3}$$

where N_C and N_V are the effective density of states in the conduction band and the valence band, respectively, and E_g is the bandgap energy. The concentration of charge carriers can be changed from its intrinsic value either by doping, which will be discussed in section 2.3.1, or through external injection, e.g. by connecting the device to a voltage source, or by illumination, which will be explained in the end of this section.

2.3.1 Charges from Doping

The intrinsic carrier concentration at room temperature is small. As an example, $n_i = 2.25 \cdot 10^6$ cm^{-3} for GaAs.[10] By addition of dopants in the material, the concentration of free charge carriers is increased. Dopants are contamination atoms which add states in the bandgap. One example of a dopant is an atom with five valence electrons, i.e. one more than is required for the covalent bonds in the crystal. The extra electron will then be loosely bound as it sees a screened potential from the atomic nucleus, and the atom is thus easily ionized. These types of dopants are called *donors* as they add electrons to the conduction band, and the material which is doped with donors is of n-type. Similarly, atoms with three valence electrons can be added to the material. In this case there is one missing electrons for the covalent bonds, which is considered as a *hole*. An electron from a neighboring atom can easily migrate and fill the state, creating a hole in the neighboring atom. These types of dopants are called *acceptors*, and the material doped with acceptor dopants is called p-type.

The energy gap between the donor/acceptor states and the conduction/valence band (illustrated as ΔE in figure 5b and 5c, respectively) is usually around the same order of magnitude as the thermal energy at room temperature. Therefore, room temperature is, in most cases, sufficient for complete ionization of the dopant states.[13] The change in electron concentration in the conduction band, Δn, is then equal to the dopant concentration, N_D, for n-type materials, and equivalently, the additional hole concentration, Δp, is equal to the acceptor concentration, N_A, for p-type materials. The free charge carriers can, as a result, contribute to a current if connected to a voltage source. It should be noted, however, that if there are no external fields, and if the material is homogeneously doped over a large volume, there will be the same concentration of ionized dopant atoms as there will be of oppositely charged, free charge carriers, resulting in a charge neutral material.

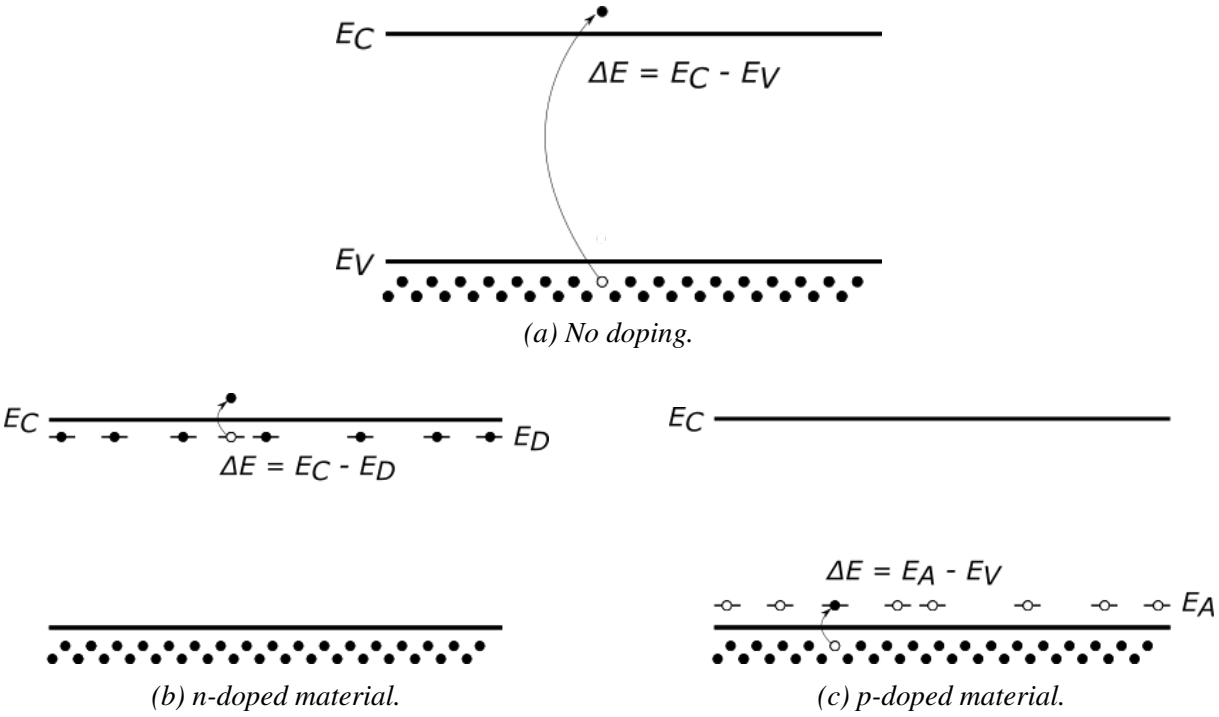

(a) No doping.

(b) n-doped material.

(c) p-doped material.

Figure 5: Energy levels of (a) an undoped, (b) an n-doped, and (c) a p-doped semiconductor material.

An undoped material have the Fermi level in the middle of the bandgap. When dopants are introduced into the material, the Fermi level is shifted. How much and in what direction is determined by the type of dopant and the concentration of it. An n-doped material will have the Fermi level shifted towards higher energy, reflecting the higher probability to have electrons in the conduction band. Similarly, the p-doped material will have a Fermi level shifted towards lower energy.

2.4 The *pn*-junction

This section is devoted to explaining the intriguing and very useful properties that originate when a p-doped and an n-doped material are in contact. This so-called *pn-junction* is used extensively in the semiconductor industry, and especially for PV-solar cells, which is the focus for this thesis. The general properties of the *pn*-junction, such as the space charge, electric field, and the potential, is presented, followed by the voltage–current characteristics of the device, and how it is affected by illumination.

2.4.1 Charge migration over the junction

One way to understand the effects of the *pn*-junction is by considering the Fermi level, which should be constant in a material under thermal equilibrium. By observing the illustration in figure 6a, where the Fermi levels have been drawn relative the conduction and valence band, it is clear that an n-doped and a p-doped material cannot be in contact while maintaining constant conduction band, valence band, and Fermi level simultaneously. Instead, the transition over the junction must result in a smooth potential change of the energy bands, such that the Fermi level keeps a constant energy on both sides of the junction, as sketched in figure 6b. The change in potential is enabled by migration of charge carriers over the junction. Due to the difference in doping between the two adjacent regions, the concentration gradients of charge carriers causes diffusion over the junction. The junction between an n-doped and a p-doped region is the most classical example, and is the case considered in this section, although any gradient of net dopants would result in similar behavior. In the case of a *pn*-junction, there is an excess of free holes on the p-doped side and an excess of free electrons on the n-doped side. Electrons diffuse from the n-side to the p-side, leaving positively ionized donors on the n-side. The electrons also fill the holes on the p-side, thus negatively ionizing the acceptor atoms. This separation of charges over the junction gives rise to an electric field which will cause a drift of the charge carriers in the opposite direction, relative to the diffusion. Thermal equilibrium of the system is reached when the diffusion and the drift contribute equally to the carrier migration over the junction.

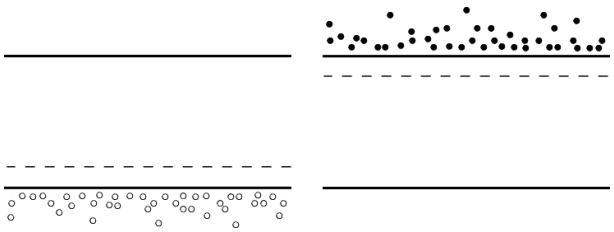

(a) Sketch of the energy bands and Fermi level of a p-doped (left) and an n-doped (right) material. Note that the relative energy gaps are not drawn to scale, but are meant to illustrate shift of the Fermi level towards the conduction band, or the valence band, depending on doping type. The extra electrons in the conduction band (filled circles), and holes in the valence band (empty circles), are due to the doping in combination with complete ionization.

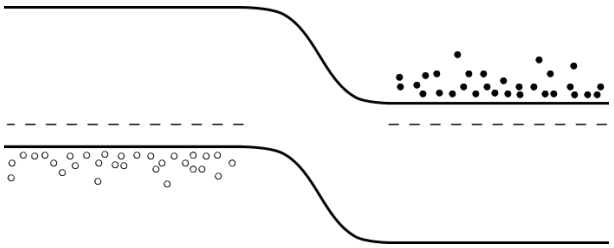

(b) When the p-doped and the n-doped materials get in contact, the concentration gradients of the charge carriers will cause a diffusion of electrons from the n-side to the p-side of the junction, and the holes from the p-side to the n-side. This separation of charges will induce an internal electric field which gives rise to a drift in the opposite direction compared to the diffusion. Equilibrium is found when diffusion and drift have equal contributions to the migration of charges over the junction.

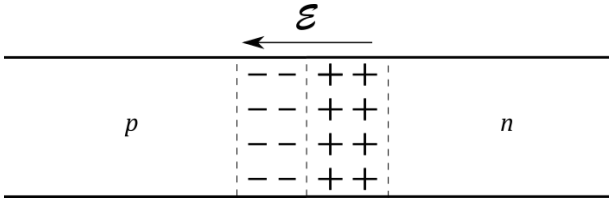

(c) The charge around the junction are due to ionized dopants, so the concentration of positive charge on the n-side will equal the concentration of donors in that region, and the concentration of negative charge on the p-side will equal the acceptor concentration.

Figure 6: Step-by-step explanation of the charge separation over the pn-junction.

2.4.2 Properties of the depletion region

The migration of charges over the junction, and the ionization of the dopant atoms, results in a region around the junction that is depleted of free charges, referred to as the *depletion region*. For an abrupt junction, the charge concentration in the depletion region, the space charge, is equal to the dopant concentration there. This is called the depletion approximation. The electric field and the potential can easily be calculated with Poisson's equation. In the

depletion approximation, this results in an electric field that is linearly decreasing on the p-side and linearly increasing on the n-side (fig. 7b), and a potential which is increasing with a quadratic behavior as can be seen in figure 7c. The equilibrium space charge will correspond to a change in potential over the junction. This potential causes a shift of the energy bands such that the Fermi level becomes constant in the material.

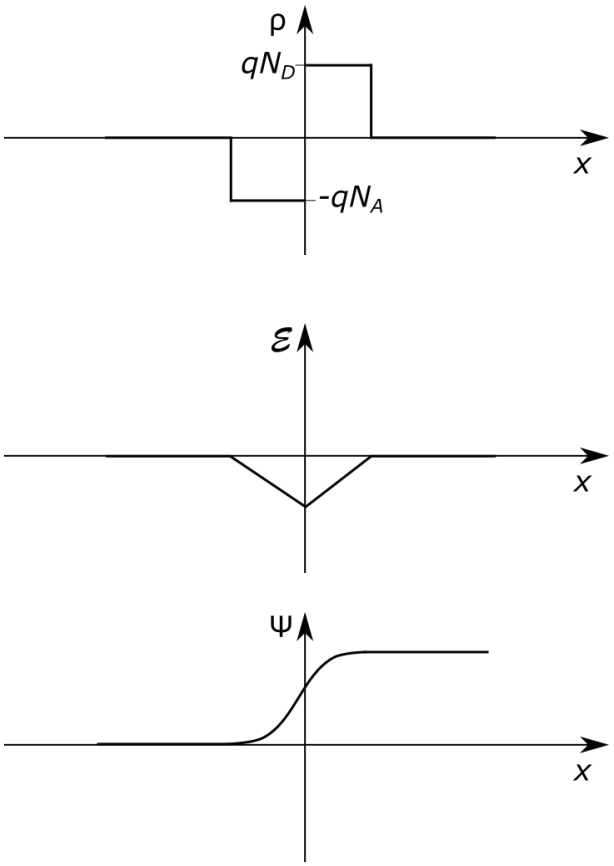

(a) The migration of charges over the junction give rise to a so-called space charge. The charge concentration on each side of the junction depends on the concentration of dopants.However, the total (negative) charge on the p-side will be equal to the total (positive) charge on the n-side, due to charge neutrality.

(b) The charge separation induces an electric field over the depletion region. For constant space charge in the different regions, the electric field will be linearly decreasing on the p-side and linearly increasing on the n-side.

(c) The charge separation also causes a shift in potential over the depletion region.

Figure 7: (a) Space charge, (b) E-field, and (c) potential for an abrupt p-n junction.

The junction might be different than the one described above, which would result in a different space charge, electric field, and potential, compared to those in figure 7. However, if one of the these characteristics are known, the other two can be calculated through Poisson's equation. The properties of the pn-region can also be manipulated, e.g., if is connected to an external voltage, or if it is illuminated. An applied bias can either add to or subtract from the potential drop over the depletion region, depending on the sign of the source. This affects the field strength over the junction and, by extension, the space charge. Similarly, if the *pn*-junction is illuminated by light with energy higher than the band gap energy, electron–hole pairs are created through excitation. If an electron–hole pair is created in the depletion region, the electric field causes

the charges to drift in opposite directions, due to their opposite signs. This effect actually acts to decrease the width of the space charge region, leading to a lower field strength and smaller potential shift over the depletion region. Since the system is not in thermal equilibrium under illumination, will the Fermi level no longer be constant through the material.

3 Part I – Modeling of nanowire dipoles

The goal of this thesis is to find the conditions in which an array of aligned and oriented NWs is obtained. A hypothesis was made that two effects occur when NWs with inherent dipoles (due to the *pn*-junctions) are exposed to a DC electric field. One of these effects is due to the interaction between the inherent dipole in the NW and the external field, which in this thesis will be referred to as the *junction dipole effect*. The NWs are not isotropic with regard to the junction dipole effect, since the direction of the dipole moment is determined by the doping concentration profile along the wire.

When any material is exposed to an external field, the charges in the material, i.e. the atomic nuclei and the electrons, will be affected. For a DC electric field, the charges will be subjected to a force in the direction of the electric field. Therefore, depending on how strongly the charges are bound, there will be some separation of charges, or polarization, in the material. Free charges will give the largest contribution to the polarization, while the atomic nuclei and bound electrons will contribute by a slight shift in the lattice. This induced charge separation from the external field will, in turn, interact with that electric field. This effect is henceforth referred to as the *polarization dipole effect*.

In the following sections, the two above mentioned effects, or interactions, are investigated. In particular, the focus has been on the relative strength of the interactions and the dependence of the electric field strength. Section 3.1 describes the general theory behind the modeling of the junction dipole and the polarization dipole. In the theory, an arbitrary one-dimensional charge distribution is considered. The following section (3.2) considers the modeled NWs and especially the charge distribution along the wires. In section 3.3, the charge distribution of the modeled NWs are incorporated into the general theory to give results on the tendency for the wires to align and orient in an applied electric field.

3.1 General theory

The NWs interact with an external electric field because they constitute of charges, i.e. ions and electrons, which are more or less tightly bound to each other. Formulas for the interaction

energy due to both the junction dipole and the polarization dipole will presented.

3.1.1 Alignment energy for an arbitrary 1-D charge distribution in an electric field

In this section the energy of a system of charges in the presence of a constant electric field is considered. The charges are regarded as a one-dimensional charge distribution for simplification, and because the modeled NWs, presented in the following section, are essentially one-dimensional.

The general expression for the electrostatic potential at a point $\boldsymbol{x}$ is given by the product between the charge concentration, $\rho(\boldsymbol{x})$, and the potential, $\Phi(\boldsymbol{x})$.[14] The potential energy of the system with one NW in the potential is obtained by integrating the product, $\rho(\boldsymbol{x}) \cdot \Phi(\boldsymbol{x})$, over the length of the NW:

$$W = \int \rho(\boldsymbol{x})\Phi(\boldsymbol{x}) d^3x \tag{4}$$

For a linear potential, given by $\nabla\Phi = -\boldsymbol{E} =$ constant, the potential can be written as a linear function of $\boldsymbol{E}$:

$$\Phi(\boldsymbol{x}) = \Phi(\boldsymbol{x_0}) - (\boldsymbol{x} - \boldsymbol{x_0}) \cdot \boldsymbol{E}$$

where x_0 is an arbitrary reference point.

Equation (4) can thus be written as:

$$\begin{aligned} W &= \Phi(\boldsymbol{x_0}) \int \rho(\boldsymbol{x})\, d^3x - \int \rho(\boldsymbol{x})(\boldsymbol{x} - \boldsymbol{x_0}) \cdot \boldsymbol{E}\, d^3x \\ &= \Phi(\boldsymbol{x_0}) \int \rho(\boldsymbol{x})\, d^3x - \Big(\int \rho(\boldsymbol{x})\boldsymbol{x} \cdot \boldsymbol{E}\, d^3x - \boldsymbol{x_0} \cdot \boldsymbol{E} \int \rho(\boldsymbol{x})\, d^3x \Big) \end{aligned} \tag{5}$$

For an object with no net charge, the following integral becomes zero:

$$\int \rho(\boldsymbol{x})\, d^3x = 0$$

This leaves an expression for the electrostatic energy that is independent of the chosen reference point:

$$W = -\int \rho(\boldsymbol{x})\boldsymbol{x} \cdot \boldsymbol{E}\, d^3x \tag{6}$$

For a NW with a charge distribution $\rho(x)$ along the wire and constant in the radial direction, that is positioned with an angle θ relative to the electric field with field strength E, equation (6) can be further simplified:

$$W_q(E,\theta) = -AE\cos(\theta)\int \rho(x)x\, dx = -Ep\cos(\theta) \tag{7}$$

where A is the cross-sectional area, and $p = A\int \rho(x)x\, dx$ is the dipole moment of the NW. Equation (7) gives the electrostatic energy of a NW, which shows a dependence of the NW dipole moment p, and on the angle θ it has to an external electric field E.

The energy gained by aligning that NW from an angle θ can be calculated by taking the difference $W_q(\theta) - W_q(0)$, which gives the following expression for the *dipole alignment energy*:

$$\boxed{\Phi_q(E,\theta) = Ep(1 - cos(\theta))} \tag{8}$$

3.1.2 Alignment energy for a polarized nanowire in an electric field

It is not only the junction dipole that interacts with an external field. An applied electric field can induce a dipole moment in the NW due to polarization of the material. This dipole will, in turn, interact with that same electric field and cause a rotation of the wire.

When a material is exposed to an electric field, polarization occurs due to an internal shift of the positive and negative charges. The polarization of a material can, in general, be separated into three parts:

- Polarization in the material in the absence of an external field, P_0, which occur for some

types of crystalline structures,

- polarization in the presence of an external field which occur due to a shift in the charges bound in the lattice, P_{latt}, and
- polarization in the presence of an external field due to a shift in the free charges (electrons) in the material, P_{el}.[15]

In this section, only the two last parts that are of interest. To simplify the calculation of the alignment energy due to polarization in the material, the NW was approximated to have an ellipsoidal ("cigar") shape. The interaction energy between a polarized NW and an applied electric field is, according to calculations done by Kim et. al.:[9]

$$W_p(E,\theta) = -\pi\epsilon_0 \, V \, E^2 \left[\frac{\cos^2\theta}{k+\kappa_1} + \frac{\sin^2\theta}{k+\kappa_2} \right] \tag{9}$$

where $\kappa_{1,2}$ are shape factors, and $k = 1/(\epsilon_r - 1)$ show the dependence of the relative permittivity. The relative permittivity is related to polarizability of the material under the influence of an external field.[15] The interaction energy depends on the volume of the NW, V, because a larger volume yields a larger amount of charge separation in the NW. W_p is proportional to the square of the field strength, E^2. The square dependence is due to the fact that the polarization of the wire and the interaction with the charge separation due to the polarization both depend on E.

The energy gained by aligning with the electric field, i.e. rotating from an angle θ to a zero angle, is:

$$\boxed{\Phi_p(E,\theta) = -\pi\epsilon_0 \, V \, E^2 \left[\frac{\cos^2\theta - 1}{k+\kappa_1} + \frac{\sin^2\theta}{k+\kappa_2} \right]} \tag{10}$$

Φ_p will henceforth be referred to as the *polarization alignment energy*.

Equation (8) and (10) can be added together to give the *total alignment energy* of the system of a NW positioned at an angle θ to an applied electric field with field strength E:

$$\boxed{\Phi_t(E,\theta) = \Phi_q(E,\theta) + \Phi_p(E,\theta)} \tag{11}$$

Equations 8, 10, and 11 are plotted in figure 11 for the model nanowires presented below.

3.2 Model nanowire

The formulas derived in section 3.1 require some information regarding the size of the NWs and their charge distribution. Below follows a description of the NWs used in the modeling and simulations in this thesis, the *model NWs*, and the method used to calculate the net charge along these wires. The model wires have same dimensions the ones used in experiments, and an approximate doping profile. The doping profile of the experimental nanowires is further discussed in section 4.1.

The model NWs are 3 µm long and have a GaAs core with a diameter of 164 nm covered with a 25 nm thick aluminum arsenide (AlAs) shell. The doping profile of the GaAs core, listed below and illustrated in figure 8, was used for the NWs since it corresponds to the target doping profile of the NWs used in the experimental part of this thesis.

Doping profile of the model NW

- 2 µm p-doped region with doping concentration $N_A = 1 \times 10^{18}\,\mathrm{cm}^{-3}$.
- 1 µm p-doped region with doping concentration $N_A = 1 \times 10^{17}\,\mathrm{cm}^{-3}$.
- 0.2 µm n-doped region with doping concentration $N_D = 3 \times 10^{19}\,\mathrm{cm}^{-3}$.

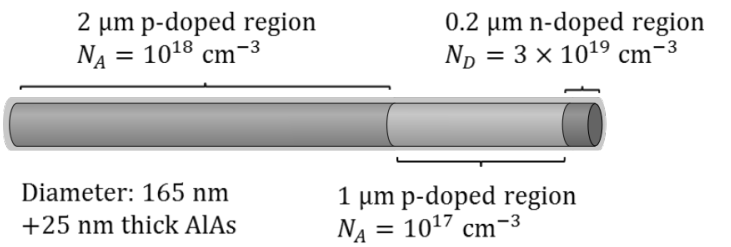

Figure 8: Doping profile of the NW

The net charge along the NWs was determined through simulations in the software Silvaco. From Silvaco information such as the potential, electric field, and concentration of electrons and holes, can be obtained. The conditions for the simulations were one sun illumination and open circuit voltage. According to the properties of the pn-junction, a one sun illumination would decrease the strength of the dipole around the junction (see section 2.4.2) and can thus be considered a worst case scenario, compared to an indoor environment or dark conditions.

3.2.1 Potential

Figure 9 shows the potential along the NW as a result from the simulation in Silvaco (stars). The x-axis shows the distance from the bottom of the NW, i.e. the p-doped end. The potential is constant except for over the two junctions: the pp-junction and the pn-junction, where there is an increase of ~ 0.1 V and ~ 0.4 V, respectively.

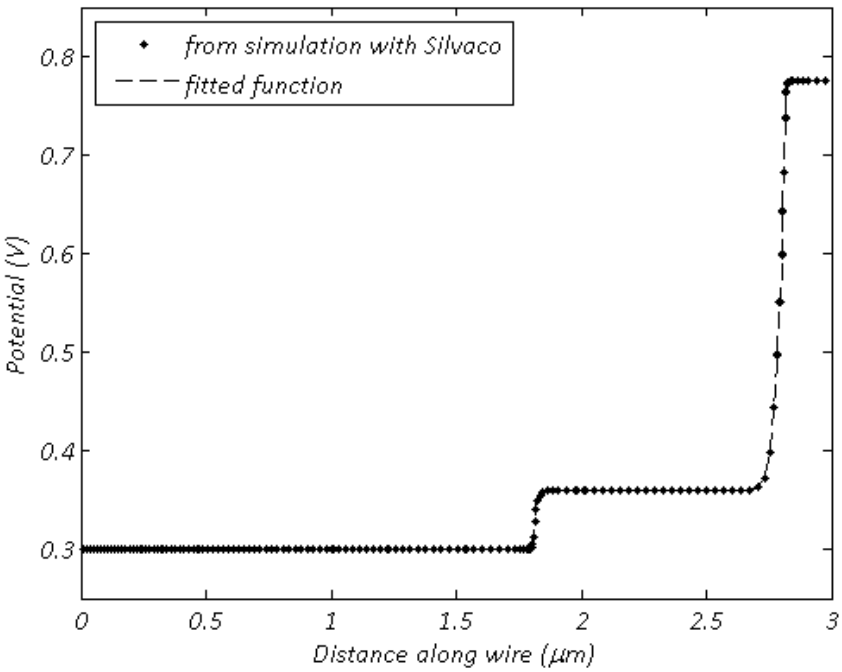

Figure 9: Potential along the model NW, from simulation (diamonds) and fitted function (dashed line).

In order to calculate the space charge along the wire, functions were fitted to the potential. The

potential, $\psi(x)$, was assumed to have the following form around junctions:

$$\psi_p(x) = \psi(x_p) + C_p(x - x_p)^{p_p}$$

$$\psi_n(x) = \psi(x_n) - C_n(x_n - x)^{p_n}$$

where $x_{p,n}$ are the points in the beginning and the end of the slope, respectively, and p_p, p_n and $C_{p,n}$ are the parameters subject to the fit (values in table 1. The following boundary conditions were also applied:

$$\psi_p(x_0) = \psi_n(x_0)$$

$$\frac{d\psi_p(x)}{dx}|_{x=x_0} = \frac{d\psi_n(x)}{dx}|_{x=x_0}$$

where x_0 is at the point where the second derivative of the slope is zero. Note that the above conditions were used for both junctions – for the first junction, the p-side should be interpreted as the side with higher concentration of p-dopants, and the n-side as the side with lower p-concentration.

Table 1: Fitted parameters.

	C_p	C_n	p_p	p_n
1^{st} (pp-)junction	$7.5 \cdot 10^{18}$	$8.5 \cdot 10^{36}$	3.7	7.5
2^{nd} (pn-)junction	$5.7 \cdot 10^{25}$	$1.1 \cdot 10^{56}$	5.5	10.5

The values of the parameters subject to the fit (listed in table 1) are uncomfortably large. However, the resulting function were tested with the coefficient of determination (R^2), which is a value that indicates how good the fit is. Both junctions got a value of R^2 above 0.99. Therefore, the values were accepted and used for the derivation of the space charge along the NW.

3.2.2 Space charge

Once an expression for the potential was obtained, the electric field and the space charge could be calculated using Poisson's equation:

$$\nabla^2\Psi(x) = -\boldsymbol{\nabla}\cdot\mathbf{E}(x) = -\rho(x)/\epsilon_0 \tag{12}$$

where $\psi(x)$ is the scalar potential, $\mathbf{E}(x)$ is the electric field, and $\rho(x)$ is the charge density along the wire.[14] The resulting expression for the electric field and the space charge have been plotted in figure 10, respectively.

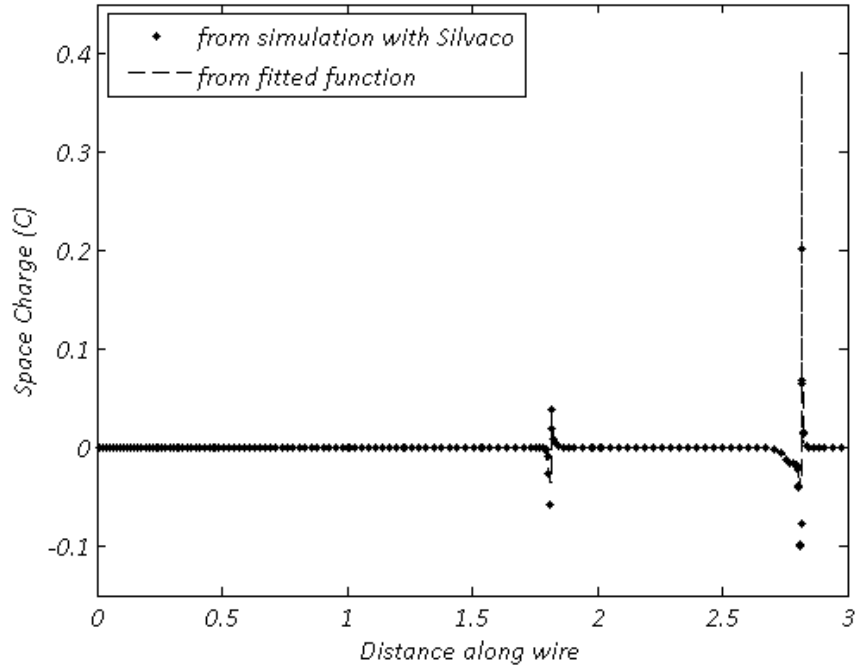

Figure 10: Simulated (diamonds) and calculated (dashed line) space charge along the model nanowire.

3.3 Modeling results for alignment energy of nanowire dipoles

Below are the results from incorporating the model NWs into the general model introduced in section 3.1. These results are used to calculate the probability of alignment and orientation of the NWs in an external electric field.

The alignment energy due to the junction dipole (eq. (8)) and the polarization dipole (eq. (10)) are plotted together with the total potential energy (eq. (11)) in figure 11 as a function of initial angle to the electric field (θ). The alignment energy is plotted in terms of thermal energy, kT, in room temperature. A zero angle indicates that the NW was aligned and oriented in the direction

of the electric field before it was applied. The angle $\theta = \pi/2$ corresponds to when the NW is perpendicular to the field, and for $\theta = \pi$ the NW is aligned, with the n-doped side pointing in the opposite direction to the electric field, i.e. the wire was aligned, but not oriented. As can be seen in the plot in figure 11, the alignment energy due to polarization is symmetric around $\theta = \pi/2$, showing that there is no directional preference for the alignment. This is in agreement with the derivation of equation 10, where the NW is assumed to be ellipsoid, and with no material variations along the wire.

The junction dipole effect shows a preferred orientation, as expected, and thus the NW obtains the largest torque when it is perpendicular to the electric field, which is the case in general for a dipole. As a result, the shape and the degree of asymmetry around $\theta = 0.5\pi$ depend on the relative strength of its two components.

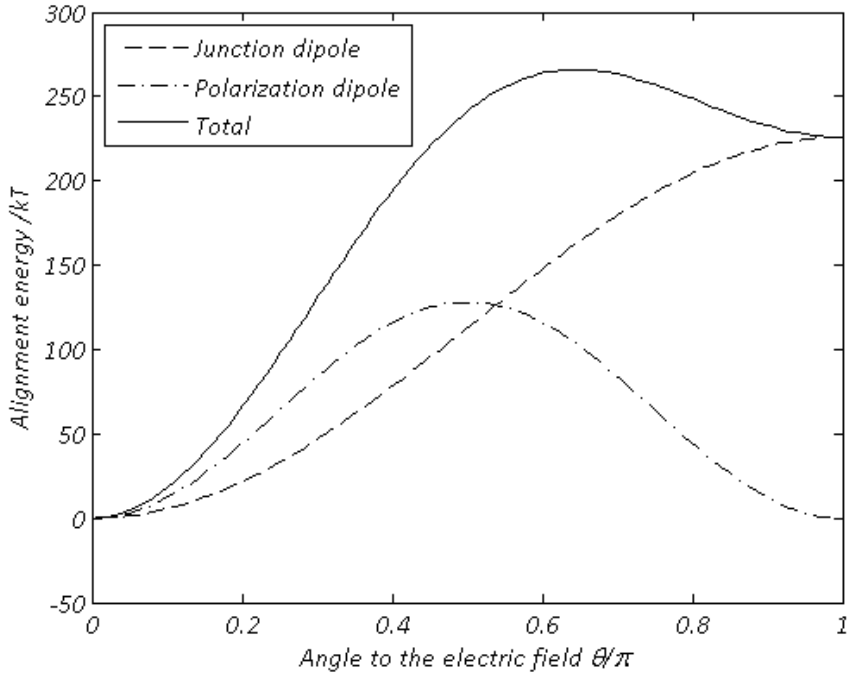

Figure 11: Junction dipole contribution (dashed line) and polarization contribution (dot-dashed line) to total alignment energy (dashed black). Electric field strength: 6 kV/cm.

The relation between the alignment energy and the applied electric field is different for the junction dipole effect and the polarization effect. The proportionalities follow:

$$\Phi_q \propto \mathrm{E} \qquad \Phi_p \propto \mathrm{E}^2$$

This implies that the junction dipole is the dominating contribution to the total alignment energy for low electric fields, while the polarization effect takes over for high field strengths. The result of this is shown in figure 12, where the total alignment energy of the model NW in the presence of different field strength strengths is plotted. As can be seen in figure 12:

- For $\mathbf{E} = 0.6$ V/μm, which is the same field strength as in figure 11, the distance between minimum and maximum for the polarization potential is about half of that of the junction dipole potential, which results in a local minimum in the total potential at $\theta = \pi$. The effect of the local minimum is that if the NW has an initial angle higher than that of the potential maximum, θ_{max}, the NW will align with opposite orientation compared to those with an angle $\theta < \theta_{max}$.

- For $\mathbf{E} = 0.2$ V/μm the plot of total potential energy has a very similar shape to that of the junction dipole effect. In addition, the derivative is positive in the whole domain $0 < \theta < \pi$, which means that it would be energetically favorable for the NW to align and orient, regardless of initial angle, θ.

- The alignment energy when $\mathbf{E} = 0.02$ V/μm has a similar shape to that of $\mathbf{E} = 0.2$ V/μm, although it is much weaker. Since the difference in potential energy between the maximum and minimum point is on the order of kT, the angular position will not be as well defined as for the two previous cases. This is visualized in the angular distribution function, plotted in the figure 13.

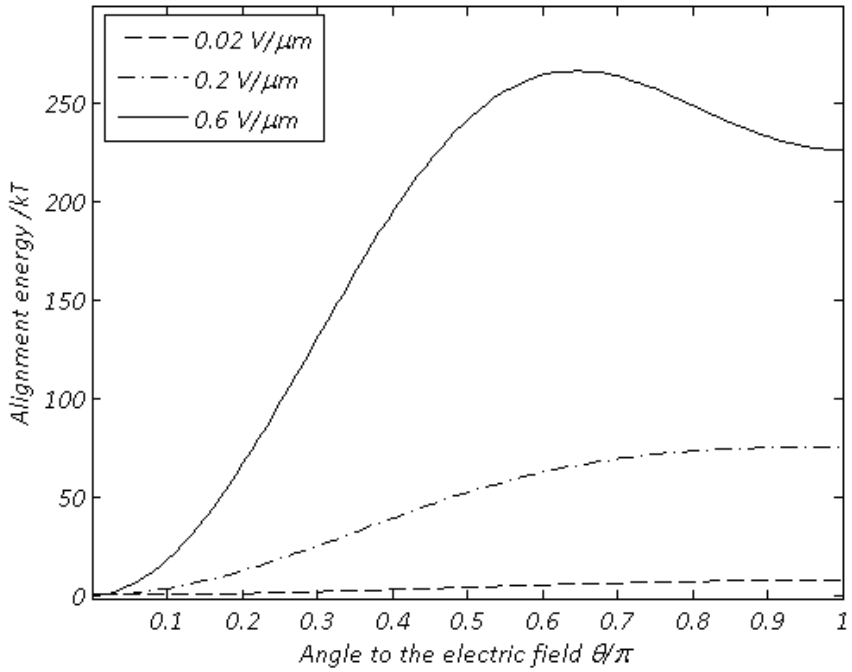

Figure 12: Total potential energy for different field strengths showing how the angular dependence change due to the relative strengths of the junction dipole and the polarization.

3.3.1 Nanowire alignment and orientation probability

The results presented above are used to calculate the distribution of angles the NWs have in an electric field with a certain field strength. The calculations are based on the assumption that the NWs have an initial random angular distribution (before E-field is applied) and that they, once the electric field is turned on, reach a Boltzmann distribution.

The probability of finding the wire within an angle θ to $\theta + \mathrm{d}\theta$ relative to the electric field, given the total alignment energy Φ_t is:[9]

$$P(\theta)\,\mathrm{d}\theta = ce^{-[\Phi_t(\theta) - \Phi_t^{min}]/kT}\sin\theta\,\mathrm{d}\theta \tag{13}$$

where c is a normalization constant. The normalization was done by assuming that the intergral of eq. 13 over the range $0 < \theta < \pi$ is equal to one:

$$\int_0^\pi P(\theta)\,\mathrm{d}\theta = c\int_0^\pi e^{-[\Phi_t(\theta)-\Phi_t^{min}]/kT}\sin\theta\,\mathrm{d}\theta = 1 \tag{14}$$

which gives us:

$$c = \left[\int_0^\pi e^{-[\Phi_t(\theta)-\Phi_t^{min}]/kT}\sin\theta\,\mathrm{d}\theta\right]^{-1} \tag{15}$$

In the cases where the function $\Phi_t(\theta)$ has a local minimum at an angle $\theta \neq 0$ equation (15) was separated into two domains of $\theta_1 = [0, \theta_{max}]$ and $\theta_2 = [\theta_{max}, \pi]$. To find the normalization constant, which in this case differs from one, the probability for the NWs to have an initial angle less than θ_{max} was calculated.

If the NW has an initial angle smaller than θ_{max}, i.e. the angle for which the potential energy has its maximum value, it will strive towards the global minimum at $\theta = 0$ in figure 12. On the other hand, for sufficiently high electric field strength, there will be a local minimum at $\theta = \pi$, i.e. for anti-parallel NWs. If the initial angle of a NW is larger than θ_{max}, it is here assumed that the NW will rotate into the anti-parallel position. This assumption is motivated since the potential difference between maximum and minimum points is much larger than kT, for all relevant values of E. For NWs with an initial angle of around θ_{max} there is some uncertainty as to in which direction it will orient. The size of this "uncertainty domain" depends on how fast the potential energy changes around the maximum point; in general, it is small. Also, since the uncertainty domain is fairly symmetrical, any uncertainties cancel out to a large degree. Therefore, this uncertainty is here disregarded.

The number of NWs with an angle θ is directly proportional to $\sin\theta$, assuming an initial random distribution of angles. The probability for a NWs to have an initial angle less than θ_{max} is thus given by:

$$P_{<\theta_{max}} = \frac{\int_0^{\theta_{max}} \sin(\theta)\,\mathrm{d}\theta}{\int_0^{\pi} \sin(\theta)\,\mathrm{d}\theta} = \frac{1-\cos(\theta_{max})}{2} \tag{16}$$

In the case where $P_{<\theta_{max}} < 1$ there will be two minima in equation (11) on each side of the maximum point at $\theta = \theta_{max}$. A global minimum $\Phi_t^{min,1}$ is found at $\theta = 0$, and a local minimum $\Phi_t^{min,2}$ at $\theta = \pi$. The complete probability distribution is then given by:

$$P(\theta)\,\mathrm{d}\theta = \begin{cases} c_1\, e^{-[\Phi_t(\theta) - \Phi_t^{min,1}]/kT} \sin\theta\,\mathrm{d}\theta & \text{for } 0 < \theta < \theta_{max} \\ \\ c_2\, e^{-[\Phi_t(\theta) - \Phi_t^{min,2}]/kT} \sin\theta\,\mathrm{d}\theta & \text{for } \theta_{max} < \theta < \pi \end{cases} \tag{17}$$

where

$$c_1 = \frac{P_{<\theta_{max}}}{\int_0^{\theta_{max}} P_1(\theta)\,\mathrm{d}\theta}$$

$$c_2 = \frac{1 - P_{<\theta_{max}}}{\int_{\theta_{max}}^{\pi} P_2(\theta)\,\mathrm{d}\theta}$$

The angular probability distribution (eq. 17) is plotted in figure 13 for electric field strength 0.02 V/µm, 0.2 V/µm, and 0.6 V/µm. Figure 13 illustrates how a higher electric field strength result in a more well defined angular position (0.2 V/µm compared to 0.02 V/µm). However, for $E = 0.6$ V/µm some of the NWs align with an angle $\theta > \theta_{max}$.

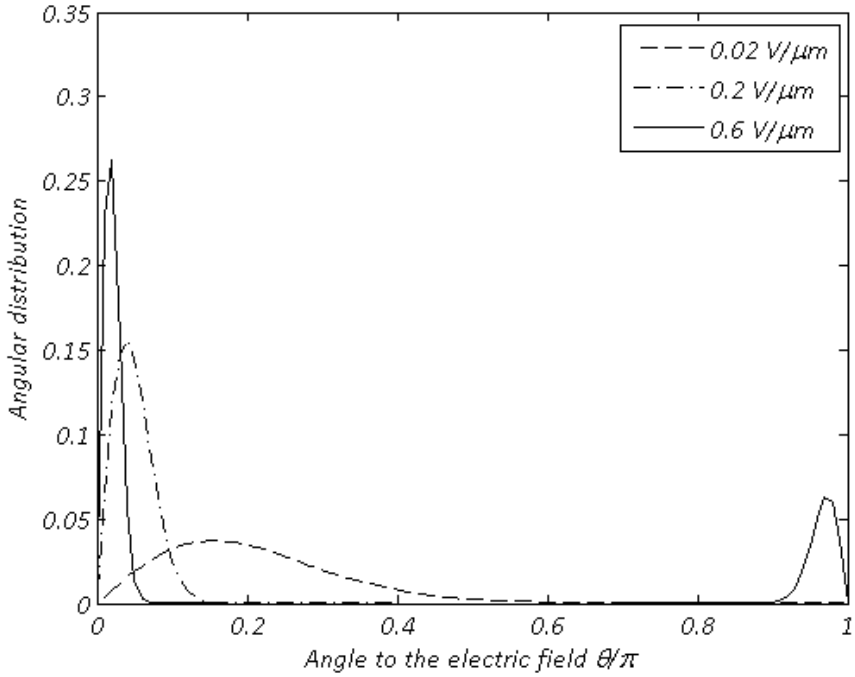

Figure 13: Angular distribution of NWs in an electric field with field strength 0.02 *V/μm (dashed line),* 0.2 *V/μm (dot-dashed line), and* 0.6 *V/μm (solid line).*

The NWs are considered to be *aligned* if they have an angle within one of the domains $0 < \theta < 0.1\pi$ or $0.9\pi < \theta < \pi$, as mentioned in section 1.2. The probability of alignment is thus calculated as:

$$P_{align} = \int_0^{0.1\pi} P(\theta)\,\mathrm{d}\theta + \int_{0.9\pi}^{\pi} P(\theta)\,\mathrm{d}\theta \tag{18}$$

Similarly, the NWs are considered as *oriented* if they have an angle within the range $0 < \theta < 0.5\pi$:

$$P_{orient} = \int_0^{0.5\pi} P(\theta)\,\mathrm{d}\theta \tag{19}$$

Finally, the NWs are *aligned and oriented* for angles $0 < \theta < 0.1\pi$:

$$P_{orient+align} = \int_0^{0.1\pi} P(\theta)\,\mathrm{d}\theta \tag{20}$$

Equations 18, 19, and 20 are plotted in figures 14, 15, and 16, respectively.

Figure 14 shows the electric field strength dependence on the fraction of aligned wires, P_{align}, i.e. NWs with an angle $\theta < 0.1\pi$ or $\theta > 0.9\pi$. There is an initial steep increase in P_{align} for increasing E, while E it is still low. This increase stops at the value of E where the fraction of oriented wires is no longer 1. This occurs at $E = 0.27$ V/μm, which can be seen figure 15 as a drop in fraction of oriented NWs from the value of one. It is NWs that are oppositely oriented that contribute to the increased fraction of NWs with an angle outside of the range for alignment.

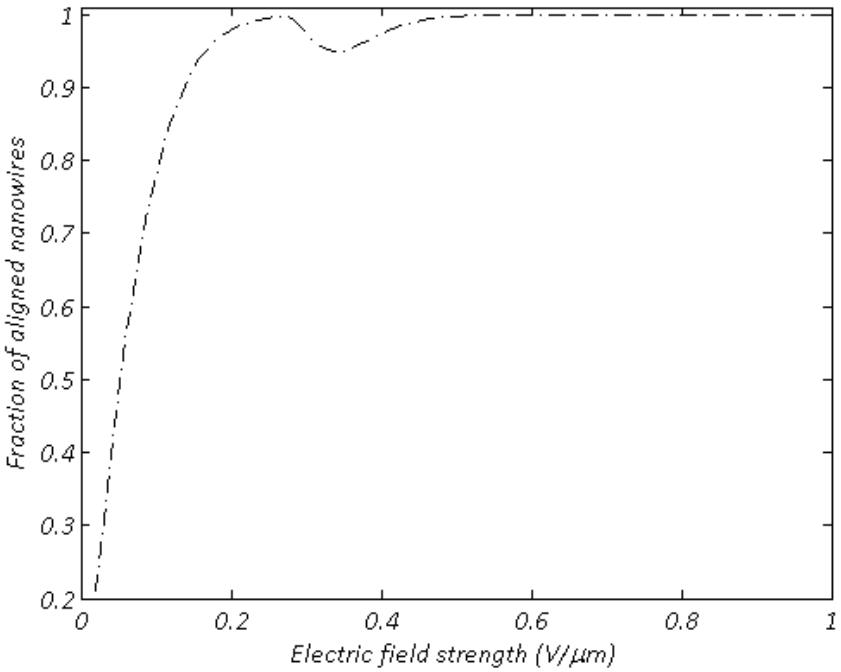

Figure 14: Fraction of aligned wires as a function of electric field strength.

The probability for orientation as a function of electric field strength is plotted in figure 15. The plot illustrates that $P_{orient} = 1$ for low field strength (expect for very low electric field, for which the angular position is not well defined). The decrease that is initiated for $E = 0.27$ V/μm is the result of the local minimum that arises in equation 11.

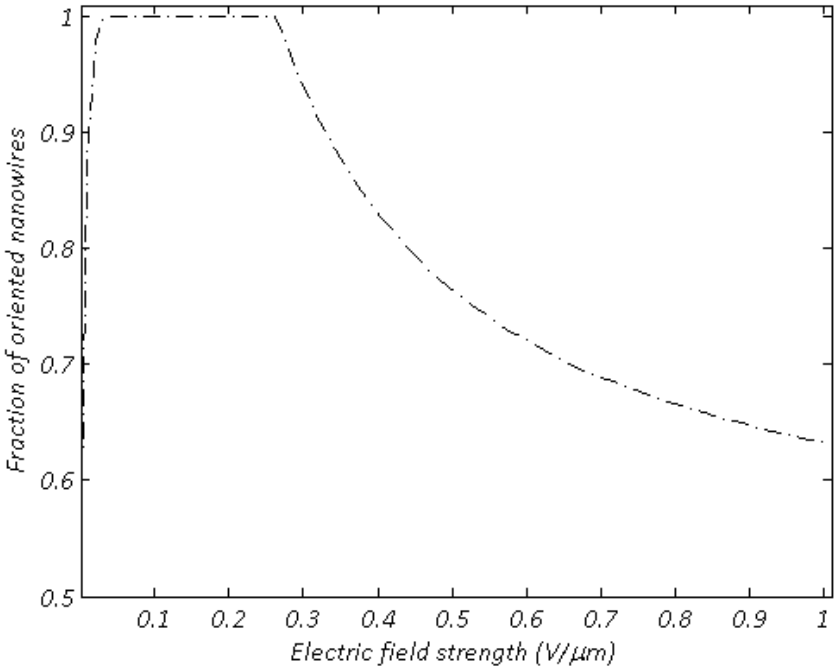

Figure 15: Fraction of oriented wires as a function of electric field strength.

Figure 16 show the fraction of NWs that end up aligned and oriented when an external electric field is applied. The plot shows that if 90% oriented and aligned wires is desired, the field strength should be kept within the domain $0.15\ \mathrm{V/\mu m} < E < 0.33\ \mathrm{V/\mu m}$. The maximum value of $P_{orient+align}$ is found for $E = 0.26\ \mathrm{V/\mu m}$ at a value of 99.4%.

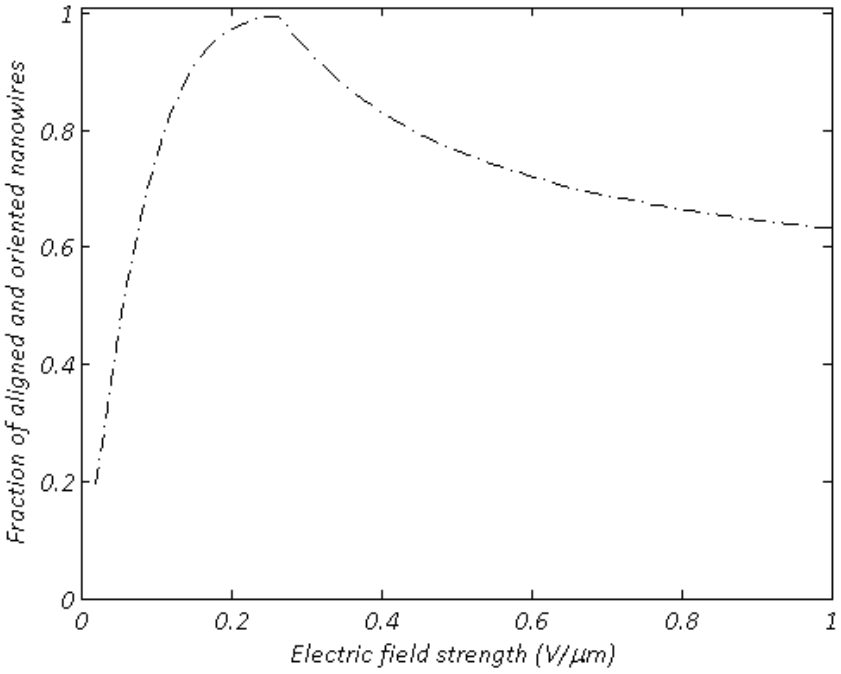

Figure 16: Fraction of aligned and oriented wires as a function of electric field strength.

The plot in figure 16 might give the appearance that this method is rather sensitive to the electric field strength, due to the narrow domain that give a large number of oriented NWs. However, it s not necessary to keep the field strength at such a low value once the NWs have rotated to an angle less than $\pi/2$. Since θ_{max} is lower than $\pi/2$, once all wires have been rotated to have an angle less than 0.5π, the field strength can be ramped up to high, without destroying orientation. This procedure should, in theory, result in 100 % aligned and oriented NWs.

4 Part II – Experimental alignment of nanowires

An experiment was designed to test dependence of the electric field strength on alignment and orientation of NWs in a dispersion. The purpose of the experiments was to collect empirical data to compare with the model presented in the previous section. An additional objective was to develop a method for producing a NW thin film. This section opens with a description of the NWs used in the experiments. Thereafter, the production method is described, followed by the methods used for characterization procedures. The final part of this section presents the experimental results along with a discussion of the results.

4.1 The nanowires

The NWs used in these experiments were grown through metal-organic chemical vapor deposition (MOCVD) that were doped – p-type (Zn) and n-type (Sn) in the opposite ends of the wires.[5] In addition, a 25 nm thick passivation layer was grown around the wires, which has the function of removing the surface states which otherwise are a problem with GaAs. The MOCVD growth is seeded from gold particles, which remain on top of the n-doped side of the NWs after the growth is completed.

The exact doping along the NWs that were used in experiments is not known. When the wires are grown with MOCVD the dopants are introduced into the chamber, along with the other growth components, in this case gallium and arsenic. The atoms adsorb onto the gold, through which it migrates by diffusion, and builds the NW on the interface between the gold particle and the substrate. The time it takes for an atom that is introduced into the chamber to become a part of the NW can vary. It depends on the time it takes for it to find its way to, and adsorb onto, a gold particle, and it depends on the diffusion time. Therefore, a switch in dopant concentration or material in the chamber does not result in an immediate and ”sharp” change of concentration/material in the grown NW. Instead there will be a gradual change. Since the concentration gradient is not known, an abrupt junction has been assumed. An abrupt junction results in a greater space charge, compared to a gradient junction. For future research, different junctions could be investigated to see how much this changes the space charge, electric field, and potential.

Note on the gold particle on the NW: The gravitational effect from the gold top has been calculated. Assuming that the gold forms a half sphere with a radius of 100 nm, which is about half of the radius of the NW, it will have a volume of $2 \cdot 10^{-15}$ cm^3, and a mass of $m = \rho V = 4 \cdot 10^{-14}$ g. The gravitational force on the gold tip is $F = m\text{g} = 4 \cdot 10^{-16}$ N, so the difference in potential energy from having the gold up relative to gold down is $U = Fx = 0.14\,kT$, where $x = 3\,\mu$m is the length of the NW. This value is small compared to the potential energy due to the junction dipole and polarization when the gold tip (i.e. the n-doped side) is directed anti-parallel to the electric field: $\Phi_t(\pi) = 75\,kT$. Therefore the effect from the gold tip is neglected in the modeling.

4.2 Producing the NW thin film

The intended application of the NW array is a solar cell. That means that the structure of aligned and oriented NWs need to be stable and possible to contact. The contacting requirement is the reason for the need for the NWs to be oriented in the same direction, and it also sets the requirement that the wires should be in the same plane. Using a curable polymer enables handling of the wires in a dispersion until a desired structure is reached, upon which the polymer can be cured to solid a thin film. The first step, before adding NWs, was to decide on which polymer to use. The resulting film should be thin, durable, and transparent. Further requirements on the film is that it should be possible to incorporate into the solar cell integration. Requirements for the polymer during before curing, is that the viscosity is right. If the liquid is too viscous it is difficult to get a thin film, and if it has too low viscosity, the turbulent flow in the polymer will prevent an ordered structure of the NWs. The polymer used in the experiments was Sylgard® 184 Elastomer, which is a heat curable polydimethylsiloxane (PDMS) elastomer. Using a heat curable polymer enabled more time to work with the experiment before the film cured and the experimental environment was not as sensitive to light, compared to when using a UV curable polymer. This polymer has a relatively high viscosity of 3500 cP when mixed,[16] which enabled good control of the film and of NWs during experiments.

The procedure of producing the film was the following:

1. A dispersion of GaAs p-n junction NWs in ethanol was added to the PDMS base, and the ethanol was allowed to evaporate before mixing in a speed mixer at 3500 rpm for 2 minutes.
2. The mix was degassed in a desiccator for a couple of minutes.
3. 200 µl of the base+NW mix was used to mix with 20 µl of initiator in the speed mixer at 3500 rpm for 2 minutes.
4. A small amount of the mix was added to a glass microscope slide with a layer of indium tin oxide (ITO), which is a transparent conductor that was used as a contact layer for the electrodes. An additional ITO-slide was applied on top of the mixture, with a lateral shift of about one centimeter. The two slides was pressed together by hand and fixed with tape.
5. The composition, illustrated in figure 17, was placed on a heating element and attached to electrodes, one to each plate.
6. The voltage was applied and stayed on during the heat program. The heat program was set to a temperature of 80 °C during 3 hours.
7. The set-up with the heating pad was positioned under an optical microscope. Images were taken of the NWs under the influence of the electric field, which was used for characterization. The characterization process is discussed in section 4.3.

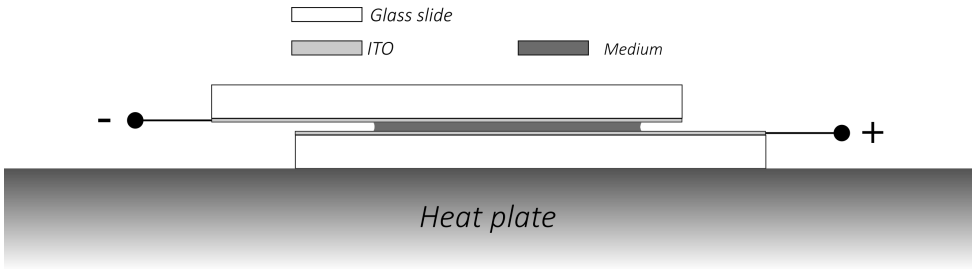

Figure 17: Sketch over the experimental set-up.

When experimenting with the optimal way to produce the thin film under the influence of an electric field, tests were performed with an additional layer of insulating material between the ITO and the polymer mixture. This procedure was done in order to to prevent short circuit between the two conducting plates, which was necessary for some polymers under the influence of high field strength. The following insulation layers were tested:

- Thin layer of polyvinyl alcohol (PVA) that had been spin coated onto the slides.
- 50 nm thick oxide layer that had been added by atomic layer deposition.
- A piece of office tape that had been attached to the glass slides.

However, for PDMS, which was used in the experiments presented in this thesis, there were no problem with short circuit at the field strengths used. Therefore, the additional insulation layer was not used.

4.3 Characterization

After the film was cured, the glass slides were separated. If the film had cured properly, it stuck to one of the slides. The characterization of the film consisted of three parts:

- the film thickness, which was necessary in order to determine the separation between the conducting plates, and thus the field strength that the wires were exposed to,
- the fraction of aligned wires and
- the orientation of the wires.

4.3.1 Film thickness

The *film thickness* was characterized by using a profilometer to do a number of scans over the edge, on different locations around the film, from which an average value was obtained. An example of such measurement is shown in figure 18. The advantage of this method is its speed and absence of required manual interaction. A weakness of the method is due to the properties of the film, which were not ideal for this tool. Because the film was quite soft, in some cases, the stylus sunk into the film and stuck during the scan, which resulted in a jagged movement and an inaccurate profile. There were also variations in thickness around the film, due to manual application of the glass slides.

Figure 18: Example of profile measurements of a film edge. The average height in the green region is compared to the average height in the red region.

4.3.2 Analysis of nanowire alignment

The *fraction of aligned NWs* was characterized by optical microscopy of the NWs in the polymer while under the influence of the applied electric field. A NW is considered to be aligned if it has an angle in the range $0 < \theta < 0.1\pi$ or $0.9\pi < \theta < \pi$ relative to the electric field line. In order to determined whether a NW was aligned, an image was taken from above with an optical microscope. The angle be determined from the apparent length of the NW in the image. An example of such image is shown in figure 19. If the NW has a very small angle, it appears as a dot in the image, and if it is perpendicular to the field lines, it appears with its true length, l_{NW}. At the limit for alignment, where $\theta = 0.1\pi$ and $\theta = 0.9\pi$, the NW has a length of $l = l_{NW} \times \sin(0.1\pi) = l_{NW} \times \sin(0.9\pi) \approx 0.3\ l_{NW}$. Therefore, in the cases where the NW was not clearly aligned or not, the length of the NW was measured. This analysis of alignment was done using the program ImageJ. For each NW thin film, 5-6 images were taken at different positions around the sample and analyzed. In total, an average of 310 NWs were counted per film.

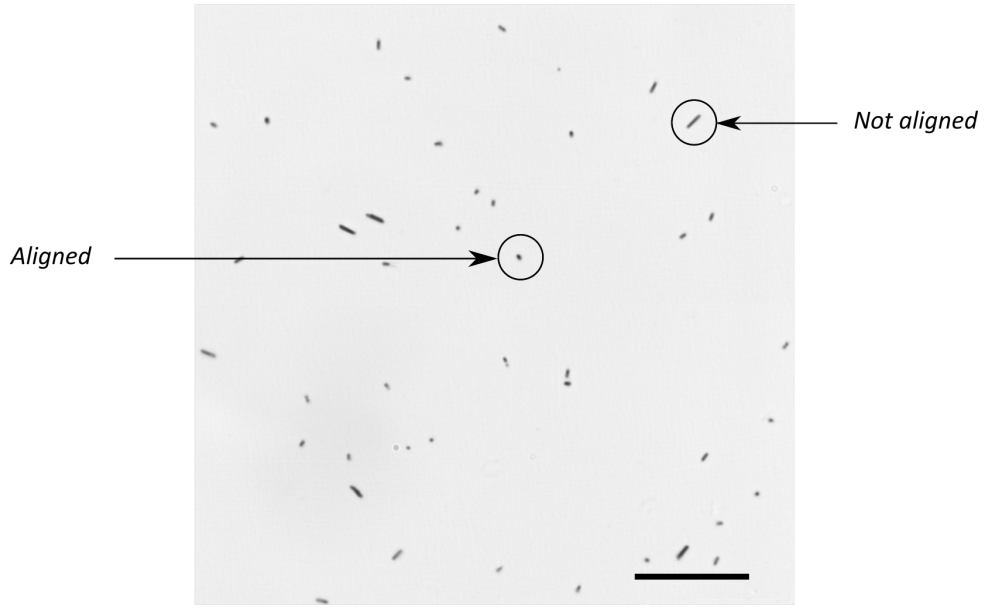

Figure 19: Optical microscopy image of NWs in PDMS before curing, under the influence of an electric field. Field strength: 1.6 V/μm. The bar corresponds to 20 μm.

A limitation of this method was the lack of depth in focus, which meant that not all NWs within the viewed region were visible simultaneously. for one region of the film, it was possible to find different set of NWs in different focal planes. This problem was solved by stacking images from varying focus depths, although at the cost of lower resolution.

4.3.3 Analysis of nanowire orientation

The most challenging and time consuming part of the characterization was determining the *orientation of the NWs*. The two ends could be distinguished due to the gold seed particle attached to the n-doped side of the NW. This difference could not be distinguished through the optical microscope. Instead, a scanning electron microscope (SEM) was used. A limitation of the SEM was that the PDMS is not transparent to the probe electrons. In order to make the NWs visible, the thin films were etched using oxygen plasma ashing, during two minutes. This removed organic material in a layer of approximately one micrometer, enabling some NWs to ”stick out” of the film and thus be visible in the SEM, as visualized in figure 20. The PDMS does not conduct electrons which resulted in charging of the material which disturbed the image. In order to reduce charging, only a small part of the film was used and attached to a conducting surface.

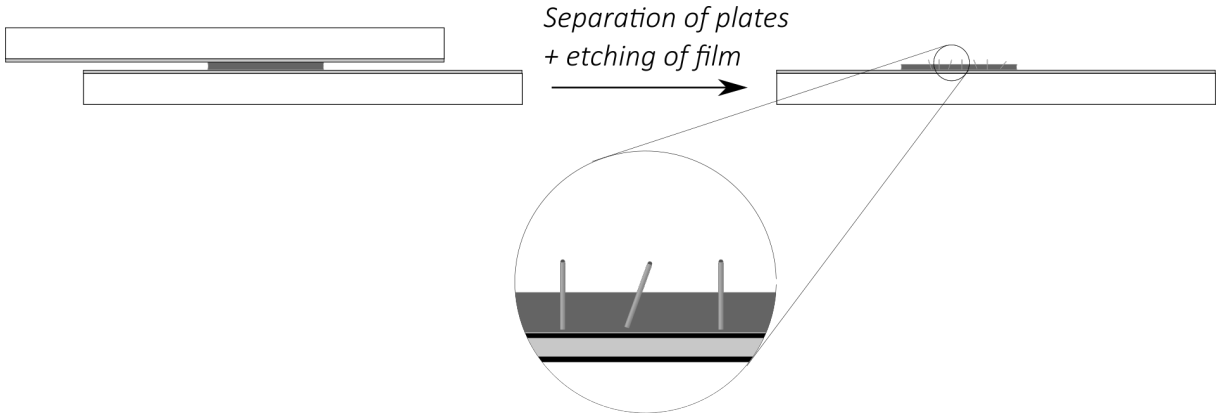

Figure 20: After the film is cured, the plates are separated and the film is etched about 1 μm such that the tips of the NWs are exposed.

The NW was regarded as oriented if the tip sticking out of the film formed a gold seed particle, as in figure 21a. In the absence of the gold seed particle, as in figure 21b, it was assumed that to gold tip was present on the opposite side, which meant that the NW was not oriented. Another explanation of the absence of the gold seed particle is that it had been detached from the NW, although, that is rather rare for the MOCVD grown NWs.

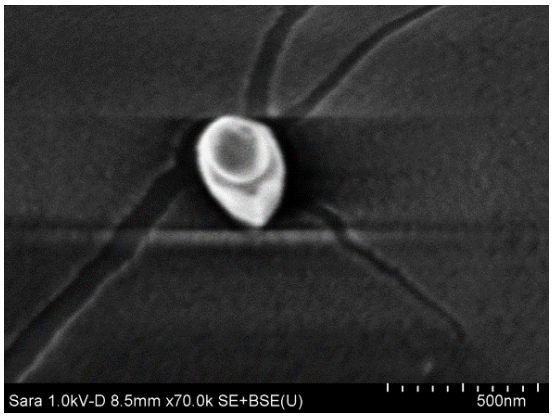

(a) Top up.

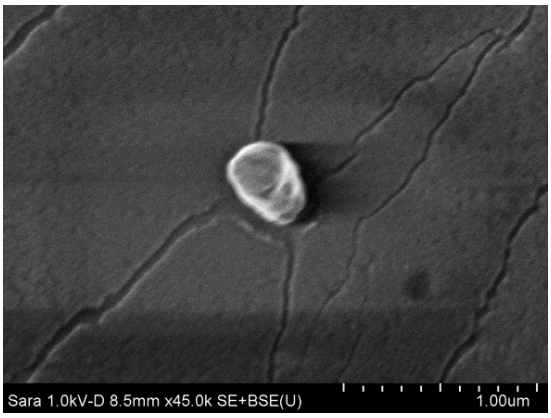

(b) Top down.

Figure 21: Two examples of SEM images of NWs in the polymer film. In these images it is fairly clear in which direction the NW is oriented from the presence (a) or absence (a) of a gold seed particle at the visible end of the NW.

4.4 Experimental results & discussion

The results from the experiments described above are summarized in two plots: one for the fraction of aligned NWs (figure 22), and one for the fraction of oriented NWs (figure 23). In

addition, the results from the modeling have been added to the plots with the experimental data. The purpose of this is to get a comparable view between the computations and experiments.

4.4.1 Nanowire alignment

The fraction of aligned NWs, illustrated in figure 22, includes the results from nine experiments, i.e. nine produced films with varying applied voltage and film thickness. Since the electric field strength could not be controlled directly, but had to be measured afterwards, it was difficult to make systematic measurements. It should also be noted that the results in figure 22 represent experiments performed over a few months. During this time the experimental process was altered and the characterization method improved. An example of such improvement is an increased efficiency of the steps after adding the initiator to the PDMS base until the set-up was complete and the electric field was applied. Also, during the optical microscopy of the first produced films, the different focal planes were not stacked. This means that, for those films, all NWs in the viewed region were not counted.

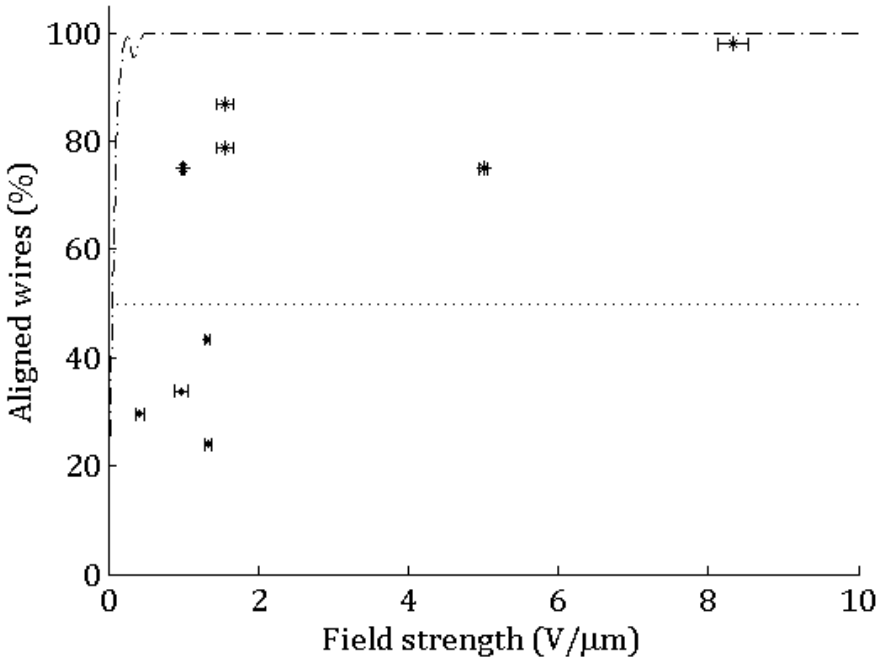

Figure 22: Fraction of aligned NWs for different applied field strengths. Each data point corresponds to one produced NW thin film. The dashed line show the modeling results.

The experimental results show much lower fraction of aligned NWs, than was predicted by numerical modeling. For the modeling, the only component that inhibited alignment was the

Brownian motion. In reality there might be additional obstacles such as adhesion to the glass slides or to other NWs. If two or more NWs are stuck together, the resulting dipole moment would be very different to that of a single NW.

4.4.2 Nanowire orientation

The experimental results for NW orientation are shown in figure 23 and consist of six data points. This characterization step required a cured film that could be etched and transferred to the SEM. This was not always achieved and, thus, there are fewer data points for the fraction of oriented NWs compared to the alignment.

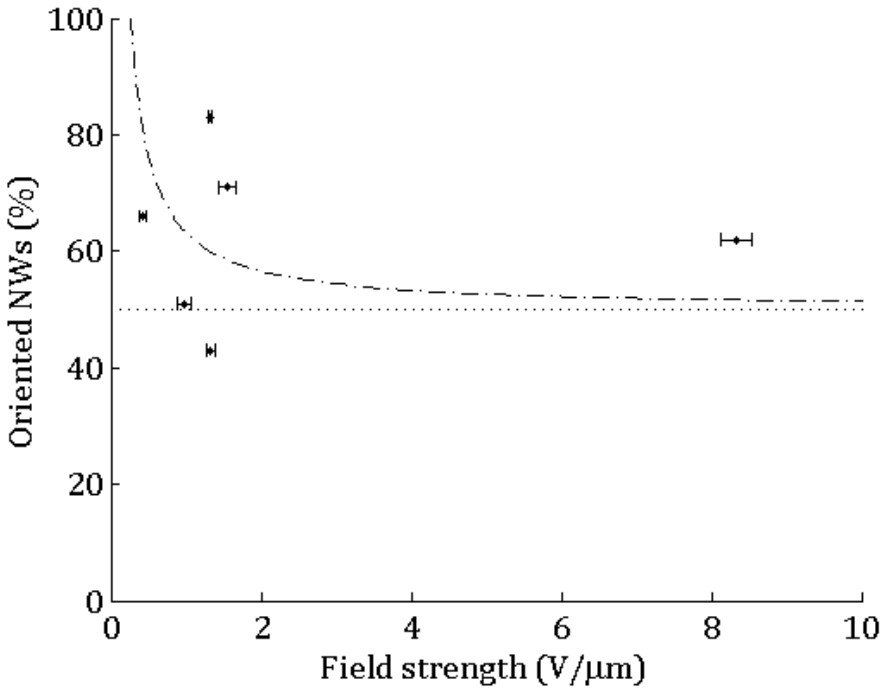

Figure 23: Fraction of oriented NWs for different external electric field strengths. Each data point corresponds to one produced NW film. The dashed line show the modeling results for comparison.

Even though the data points in figure 23 do not follow a trend that can be compared to the modeling results, there is a strong indication on a preferred direction of the NWs. The comparison between the modeling and experimental results makes it clear that the field strengths used in experiments were too high. It was shown in section 3.3 that the field strength should not be higher than 0.33 V/μm in order to reach more than 90 % orientation. However, this is true for an electric field that instantaneously reaches its final value. If the field strength was gradually

increased, all NWs could become oriented, i.e. have an angle $\theta < 90$ °C, before increasing further to obtain alignment. In this case, the degree of orientation would no longer depend on the final strength of the electric field. How slow the ramping must be depends on the rotational speed of the NW under the influence of the electric field.

4.4.3 General discussion

Some aspects of the experimental procedure that would benefit from alteration. These include:

- film quality,
- etching time,
- characterization methods, and
- environmental control.

The quality of the NW film was unsatisfactory both in terms of curing reliability and, in the cases the film did cure, durability. The curing reliability would probably be enhanced if larger quantities of the polymer mixture was used, because the small amounts used here make the relative error larger which results in incorrect proportions between the polymer base and initiator. Optimization work on mixture ratios, curing time and curing temperature would probably result in a more reliable and durable film.

The etching time is related to the characterization method. If more material was etched off, more NWs would be visible in the SEM. On the other hand, if the film was etched for too long, the the film would become fragile and difficult to work with.

Control of the environment such as ambient light during the experimental steps before the film is cured is important if the effect from light is significant. This is an effect that would be interesting to explore. Additional improvements that could make the experimental procedure more efficient would be to use an UV-curable polymer instead of heat curing. To decrease the time to cure the thin film is crucial to get a good amount of data to work with.

5 Conclusions and outlook

According to the modeling of the NW dipoles, there is a small range of field strengths for which we get close to 100 % aligned and oriented NWs. However, it turned out to be experimentally difficult to reach a high fraction of alignment and orientation simultaneously. Low electric field strengths were required to achieve oriented NWs, while alignment required higher field strengths. The proposed solution to this problem is gradual increase of the field strength. This would allow the NWs to become oriented before the field strength become high enough to form the second minimum in the alignment energy, visible in figure 12. Once rough orientation is achieved, the field strength can be increased to the level necessary for alignment of the NWs.

The next steps for the investigation of pn-junction NWs in an electric field would be:

- to compare a gradual increase of the electric field strength with an instantaneous switch on,
- measurements on the rotational speed of the NWs, in order to determine the appropriate ramping of the electric field strength,
- to explore the influence of light on the nanowires, and
- investigation of the doping profile of the NWs.

The effect of light should have an inhibiting effect on the orientation of the nanowires since it would decrease the potential difference over the pn-junction and, by extension, the dipole strength. Since electron–hole pairs are generated throughout the whole NW under illumination, there would be more free charges in the material which would increase the dipole from pollarization. I do not know how large these two effects would be, although it would be interesting to investigate.

The doping profile of the NWs used here in experiments differ from the model NWs, as discussed in section 4.1. The concentration of dopant atoms along the NWs, and in particular around the junctions, play a vital role for the momentum experienced by the NWs in the external electric field. An investigation of the true doping profile of the NWs is therefore motivated.

References

[1] ©Fraunhofer ISE: Photovoltaics Report (2014) Updated: 28 July 2014.

[2] APS Physics. (2009). April 25, 1954: Bell Labs Demonstrates the First Practical Silicon Solar Cell. [ONLINE] Available at: `http://www.aps.org/publications/apsnews/200904/physicshistory.cfm`. [Accessed 19 February, 2016].

[3] Jha, A.R. (2010). *Solar Cell Technology and Applications*, Taylor and Francis Group, Boca Raton, FL.

[4] SolFilm™, A Lot More Power. [ONLINE] Available at: `http://solvoltaics.com/solink.shtml`. [Accessed 5 February, 2016].

[5] Åberg, I., Vescovi, G., Asoli, D., Naseem, U., Gilboy, J., Sundvall, C., Dahlgren, A., Svensson, K.E., Anttu, N., Björk, M.T., Samuellson, L. (2016). A GaAs Nanowire Solar Cell With 15.3% Efficiency at 1 Sun. *IEEE Journal of Photovoltaics, Vol. 6, No. 1*.

[6] Heurlin, M., Magnusson, M.H., Lindgren, D., Ek, M., Wallenberg, R., Deppert, K., Samuelson, L. (2012). Continuous gas-phase synthesis of nanowires with tunable properties. *Nature, Vol. 492*.

[7] Crassous, J.J., Mihut, A. M., Wernersson, E., Pfleiderer, P., Vermant, J., Linse, P., Schurtenberger, P. (2014). Field-induced assembly of colloidal ellipsoids into well-defined microtubules. *Nature Communications, 5, 5516*.

[8] Troppenz, T., Kuijk, A., Imhof, A., van Blaaderen, A., Dijkstra, M., van Roij, R. (2015). Nematic ordering of polarizable colloidal rods in an external field: theory and experiment. *Phys.Chem.Chem.Phys., 17, 22423*.

[9] Kim, S.H., Mulholland, G.W., Zachariah, M.R. (2007). Understanding ion mobility and transport properties of aerosol nanowires. *Journal of Aerosol Science, 38, 823– 842*.

[10] Sze, S.M. (1998), *Physics of Semiconductor Devices*, 2dn edn, John Wiley & Sons, New York, NY.

[11] Kittel, C. (2005), *Introduction to Solid State Physics*, 8th edn, John Wiley & Sons, Hoboken, NJ.

[12] Zimmermann, H. (2010), *Integrated Silicon Optoelectronics*, 2nd edn, Springer-Verlag Berlin Heidelberg.

[13] Sze, S.M. (1985), *Semiconductor Devices: Physics and Technology*, 2dn edn, John Wiley & Sons, New York, NY.

[14] Jackson, J.D. (1999), *Classical Electrodynamics*, 3rd edn, John Wiley & Sons, Hoboken, NJ.

[15] Wood, C., Jena, D. (2008), *Polarization Effects in Semiconductors: From Ab Initio Theory to Device Applications*, Springer Science+Business Media, LLC, New York, NY.

[16] Dow Corning. (2014). *Sylgard 184 Silicone Elastomer*. [ONLINE] Available at: `http://www.dowcorning.com/DataFiles/090276fe80190b08.pdf`. [Accessed 20 January, 2016].